SPHERIC 2023

Rhodes, Greece, 27-29 June

Proceedings of the 17th International SPHERIC Workshop

Editor
Georgios Fourtakas
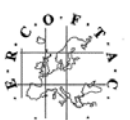
SPHERIC 2023

Proceedings of the 17th International SPHERIC Workshop

Rhodes Island, Greece, 27-29 June 2023

Editor
Georgios Fourtakas

Acknowledgements

Foreword

Dear Delegate,

Since its conception in 2005 with the Inaugural Meeting in Chatou, France, the Smoothed Particle Hydrodynamics rEsearch and Engineering International Community (SPHERIC) has foster, steered and disseminated the development and application of the Smoothed Particle Hydrodynamics (SPH) method in academia and industry alike.

The International SPHERIC Workshops are a unique series of yearly events with exclusive focus on the SPH method and associated particle-based methods. SPH has been widely adopted in the field of computational fluid mechanics, solid mechanics, geomechanics, manufacturing engineering and many other disciplines. The SPH scheme is considered to be the mainstream method for free-surface flows, and multi-phase flows, high non-linear deformation, fracture and fragmentation and, complex physics due to its meshless particle-based nature.

The SPHERIC workshop brings together state-of-the-art developments from academia and novel interdisciplinary applications from industry in a unique blend towards the advancement of the numerical scheme.

It is our pleasure and privilege to host the 17th edition of the International SPHERIC Workshop in Rhodes Island, Greece and I am looking forward to welcoming you for a stimulating and fruitful event.

Sincerely,

Georgios Fourtakas
Chair of the Local Organizing Committee
17th International SPHERIC Workshop

Committees

Scientific Committee

Prof. Renato Vacondio (Università di Parma, Italy)

Prof. Antonio Gil (Swansea University, UK)

Prof. Raj Das (RMIT University, Australia)

Prof. Ben Rogers (University of Manchester, UK)

Dr. Georgios Fourtakas (University of Manchester, UK)

Dr. Chun Hean Lee (Universiy of Glasgow, UK)

Prof Alex Crespo (Universidade de Vigo, Ourense, Spain)

Prof. Abbas Khayyer (Kyoto University, Japan)

Prof. David Le Touzé (Ecole Centrale de Nantes, France)

Dr Nathan Quinlan (National University of Ireland, Galway, Ireland)

Dr. Xiangyu Hu (Technical University of Munich, Germany)

Dr. Pengnan Sun (Sun Yat-sen University, China)

Dr. Tom De Vuyst (University of Hertfordshire, UK)

Dr Christopher Curtis Long (Los Alamos National Laboratory, USA)

Prof. Moncho Gómez-Gesteira (Universidade de Vigo, Spain)

Prof. Xu Fei (Northwestern Polytechnical University, China)

Dr. Rouhollah Fatehi (Persian Gulf University, Iran)

Dr. Nathaniel Albert Trask (Sandia National Laboratories, USA)

Prof. Mehmet Yildiz (Sabanci University, Turkey)

Prof. Andrea Colagrossi (CNR-INM, Italy)

Dr. Matthieu De Leffe (Siemens Digital Industries, France)

Dr. Salvatore Marrone (CNR-INM, Italy)

Prof. Peter Eberhard (University of Stuttgart, Germany)

Dr. Steven Lind (University of Manchester, UK)

Mr. Pierre Sabrowski (Dive Solutions, Germany)

Dr. Giuseppe Bilotta (Istituto Nazionale di Geofisica e Vulcanologia, Italy)

Dr. Ha Bui (Monash University, Australia)

Prof. Stefano Sibilla (Università di Pavia, Italy)

Prof. Antonio Souto Iglesias (UPM, Spain)

Dr Angelo Tafuni (New Jersey Institute of Technology, US)

Local Organising Committee

Dr Georgios Fourtakas

Dr Steven Lind

Dr Abouzied Nasar

Mr Chunze Cen

Mr Ruofeng Feng

Miss Meixuan Lin

Mr Sumanta Laha

Table of contents

Multiple continua and multi-phase flows

Free surface and moving boundaries

Solids and structures

Complex flows I

Geotechnical & disaster applications

Process & manufacturing engineering applications

Complex flows II

SPH simulations of sloshing flows close to the critical depth

Andrea Bardazzi[(a)], Claudio Lugni[(a)], Danilo Durante[(a)], Andrea Colagrossi[(a),(b)]

(a) CNR-INM Institute of marine engineering, National Research Council, Rome, Italy

(b) Ecole Centrale Nantes, LHEEA research dept. (ECN and CNRS), Nantes, France

danilo.durante@cnr.it

Abstract—In the present paper, the sloshing flow in a squared $L \times L$ tank is investigated with both experimental and numerical approaches. The filling depth chosen is $h/L = 0.35$ which is close to the critical depth $h/L = 0.3374$. The experimental tank has a breadth of $0.1L$ such reducing three-dimensional effects. Hi-resolution digital camera and capacitance wave probes are used for time recording of the wave height. By varying the oscillation period and the amplitude of the imposed sway motion of the tank, several scenarios in terms of free surface evolution are identified. Periodic and quasi-periodic regimes are found for the most part of the analysed frequencies but, among them, sub-harmonic regimes are also identified. Energetic chaotic regimes are found at larger amplitude motion. For the numerical investigation an advanced and well established Smooth Particle Hydrodynamics (SPH) method is used to help the comprehension of the physical phenomena involved and to extend the range of frequencies experimentally investigated.

I. Introduction

Sloshing is a resonant fluid motion that appears within a tank forced to oscillate. Because of the high local and global loads associated with the wave impact against the lateral wall, sloshing flows have several implications from the practical point of view. For example, in the naval framework the knowledge of the flow features occurring during the violent liquid motion within confined spaces [31], is a key issue for the safety of LNG (Liquid Natural Gas) carriers. Since these ships operate at different filling conditions of their tanks, it is important to gain an in-depth understanding of the main features of the involved phenomena. In particular, the filling height of the tank may drastically change the observed regimes when the the tank is almost fully [30], partially [13], or barely filled [8].

Although proper modeling of the local evolution of the flow field is fundamental for the description of the fluid loads, it is also extremely important to consider the global features of the flow during the tank motion.

Generally speaking, in sloshing flows induced by purely periodic swaying tanks, the free surface moves with a period that is strictly connected with the excitation frequency. As this latter approaches to resonant conditions, super-harmonic components, induced by the nonlinear effects, appear. Beside this, the identification of peculiar non-linear sloshing flow behaviours as sub-harmonic or chaotic modes requires the analysis of several conditions varying the filling-heights, the amplitudes and the frequencies of the tank motion.

That approach was adopted during the early experimental campaign at CNR-INM (formerly INSEAN) in 2003. The experimental setup of a similar campaign carried out in the '70s by [29] was reproduced. The same size of the tank, *i.e.* squared $L \times L$ with $L = 1$m, and the same filling depth, *i.e.* $h/L = 0.35$ close to the critical one, were considered. As in [29], in order to limit the 3D effects, the breadth of the tank was set equal to $0.1L$. In [29] the wave height was measured with a wire probe positioned ad 5 cm from one of the vertical tank sides. Beside this, in the CNR-INM campaign other three wire probes were used.

During each test a sinusoidal sway motion was imposed to the tank with a prescribed amplitude and frequency. A span of several frequencies and amplitudes was investigated through the analysis of the wave height, measured locally by the wire probes and globally by video recording. Following the experimental procedure detailed in [29], 300 seconds of motion were recorded for attaining a stable regime condition.

Following the same investigation of [12], in the present work a more accurate analysis of the wave height is carried out for $A = 0.01L$ and $A = 0.03L$, by considering the time signals of different wave probes in the proximity of the two vertical walls of the tank. Besides the values of maxima took into account by [29], the entire time history of the wave elevation is investigated, identifying the regimes attained by the flow motion.

Similarly to [15], where the identification of regimes for the flow past a NACA profile or a circular cylinder was considered, periodic monochromatic, non-monochromatic, quasi periodic and chaotic regimes are found. Moreover, as remarked in [22], for some values of the oscillation frequency, the nonlinear nature of the time signals may trigger the onset of sub-harmonics or super-harmonics that lead to doubling-frequency or tripling-period bifurcations.

In the present analysis, the experimental data obtained for $A = 0.03L$ are compared with numerical simulations obtained with δ-LES-SPH model. The reliability of δ-LES-SPH for these kind of problems comes from many validations carried out in the framework of violent sloshing flows simulations in [24]. In the present work, a large numerical campaign is performed for completing the experimental database with a wider frequency range and a larger number of analyzed frequencies. In order to investigate the effect of the motion
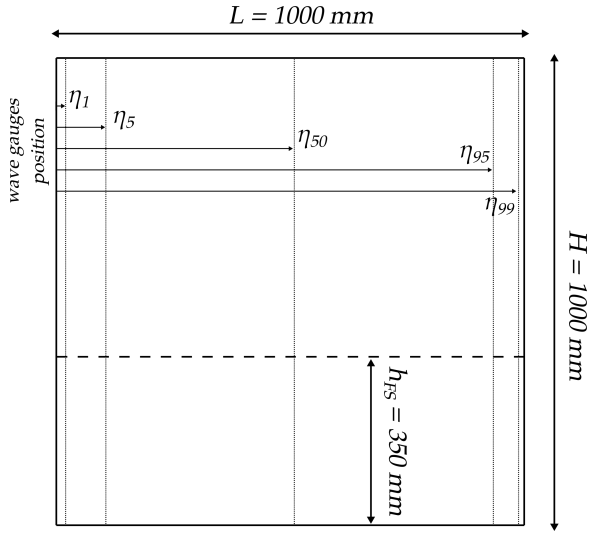
Figure 1.   Experimental box sketch with highlight of the filled volume.

amplitude, a lower amplitude database ($A/L=0.01$) is also provided, where similar analyses were performed.

II. Experimental Set-up

The tank used during the experimental campaign at CNR-INM is $L = 1$ m long and tall, $D = 0.1$ m wide and is filled with water up to $h_{FS} = 0.35$ m. The total mass of the liquid is therefore equal to $m_l = 34.76$ Kg. Based on the filling height h_{FS} selected, the natural sloshing periods can be derived from ([18]):

$$T_n = \frac{2\pi}{\sqrt{\frac{gn\pi}{L} \tanh \frac{n\pi h_{FS}}{L}}} \qquad n = 1, 2, \ldots \qquad (1)$$

by setting n equal to the desired mode. For example, by considering that g is the gravitational acceleration, the period of the first mode is $T_1 = 1.265$ s.

In order to ensure a purely sinusoidal sway motion, $x(t) = A \sin (2\pi t/T)$, an *ad-hoc* mechanical system was designed. A and T are the amplitude and the period of the prescribed motion, respectively. The small breadth of the tank, *i.e.* $D = 0.1$ m, provides an almost two-dimensional flow in the sloshing plane. Moreover, five capacitance wire probes are placed within the tank. The first two are located at a distance of 1 cm and 5 cm from the left side. Other two probes are positioned symmetrically at the right side, while the last wire probe is in the middle of the tank (*i.e.* 50 cm from the sides of the tank). The corresponding dimensionless measurements of the wave heights h_i are indicated as $\eta_i = (h_i - h_{FS})/L$ with $i = 1, 5, 50, 95, 99$.

During the tests, flow visualizations are obtained through a digital video camera JAI CV-M2. This camera has a spatial resolution of 1600×1200 pixels and a frequency rate equal to 15 Hz. It is placed in front of the tank and far enough from it to record the whole flow pattern. A wire potentiometer has been used for the evaluation of the tank position.

A suitable synchronizer is used to trigger the start of all acquisition systems, which are characterized by different sampling rates. A sketch of the experimental setup is given in figure 1.

III. Numerical solver

In the present work a two-dimensional fluid domain Ω is considered with its boundaries which are composed by the tank walls $\partial\Omega_B$ and the free surface $\partial\Omega_F$. Only the liquid phase is consider and the latter is model as a weakly-compressible media and assumed to be barotropic. The liquid is assumed to be Newtonian and the flow isothermal, while the surface tension effects are neglected. The tank translate along the x-axis and the equation are formulated in the non-inertial frame of reference (Ni-FoR). With these assumptions the δ-LES-SPH model presented in [3] and [25] is considered, *i.e.*:

$$
\begin{cases}
\dfrac{d\rho_i}{dt} &= -\rho_i \displaystyle\sum_j (\boldsymbol{u}_{ji} + \delta\boldsymbol{u}_{ji}) \cdot \nabla_i W_{ij} V_j + \\
& \quad + \displaystyle\sum_j (\rho_j \, \delta\boldsymbol{u}_j + \rho_i \, \delta\boldsymbol{u}_i) \cdot \nabla_i W_{ij} V_j + \mathcal{D}_i^\rho \\
\rho_i \dfrac{d\boldsymbol{u}_i}{dt} &= \boldsymbol{F}_i^p + \boldsymbol{F}_i^v + \boldsymbol{g} - a_{tank}(t)\,\boldsymbol{e}_1 + \\
& \quad + \rho_0 \displaystyle\sum_j (\boldsymbol{u}_j \otimes \delta\boldsymbol{u}_j + \boldsymbol{u}_i \otimes \delta\boldsymbol{u}_i) \cdot \nabla_i W_{ij} V_j \\
\dfrac{d\boldsymbol{r}_i}{dt} &= \boldsymbol{u}_i + \delta\boldsymbol{u}_i, \quad V_i(t) = m_i/\rho_i(t), \quad p = c_0^2(\rho - \rho_0)
\end{cases}
$$
$$(2)$$

where the index i refers to the considered particle and j refers to neighbour particles of i. The vectors $\boldsymbol{F}_i^p$ and $\boldsymbol{F}_i^v$ are the pressure and the net viscous force acting on the particle i. The notation $\boldsymbol{u}_{ji}$ in (2) indicates the differences $(\boldsymbol{u}_j - \boldsymbol{u}_i)$ and the same holds for $\delta\boldsymbol{u}_{ji}$ and $\boldsymbol{r}_{ji}$. The spatial gradients are approximated through the convolution with a kernel function W_{ij}. Following [3], a C2-Wendland kernel is adopted in the present work.

In order to recover regular spatial distribution of particles and consequently accurate approximation of the SPH operators a Particle Shifting Technique (PST) is used (see also *e.g.* [21, 27]). For the sake of brevity the specific law adopted for the shifting velocity $\delta\boldsymbol{u}$ is not reported here, this being identical to the one adopted by [24, 26] in which violent sloshing problems were studied.

The time derivative d/dt used in (2) indicates a quasi-Lagrangian derivative since the particles are moving with the modified velocity $(\boldsymbol{u}+\delta\boldsymbol{u})$ and the first two equations of (2) are written following an Arbitrary Lagrangian-Eulerian approach. Because of this, the continuity and the momentum equations contain terms with spatial derivatives of $\delta\boldsymbol{u}$ (for details, the interested reader is referred to [5]).

The mass m_i of the $i-$th particle is assumed to be constant during its motion. The particles are set initially on a Cartesian lattice with spacing Δr, and hence, the volumes V_i are initially set as Δr^2. The particle masses m_i are calculated through the initial density field (using the equation of state and the initial

pressure field). While the particle masses m_i remain constant during the time evolution, the volumes V_i change in time accordingly with the particle density (see bottom line of eq. (2)).

In eq. (2) a simple linear state equation linking the pressure with the density is assumed where c_0 plays the role of a constant speed of sound of the liquid and ρ_0 is the density at the free-surface (where p is assumed to be equal to zero). The weakly-compressible hypothesis implies the following requirement:

$$c_0 \gg \max\left(U_{max}, \sqrt{\frac{(\Delta p)_{max}}{\rho_0}}\right) \qquad (3)$$

where U_{max} and $(\Delta p)_{max}$ are, respectively, the maximum fluid speed and the maximum pressure variation expected (with respect to the zero pressure free-surface level) in Ω. By considering that the time integration is performed with a time step related to the value of c_0, the latter is always set lower than its physical counterpart. The constraint (3), however, must be checked for guaranteeing the fulfillment of the weakly-compressible regime.

In the present paper, the whole set of numerical simulations spans from Re=3×10^4 to Re=3×10^5, where the Reynolds number is defined as:

$$Re = \frac{2\pi\,A}{T}\frac{L}{\nu_w}$$

where $\nu_w = 10^{-6}\ m^2/s$ is the kinematic viscosity of the water, A is the amplitude of tank oscillation, T the excitation period and L the tank length (1 meter in the present investigations). By considering the Reynolds numbers involved, a sub-grid model is needed. A simple LES with a classic Smagorinsky model was adapted in the present SPH using quasi-Lagrangian formalism introduced in [3].

To avoid instabilities on the pressure field the diffusive term $\mathcal{D}_i^\rho$, introduced by [2], is added in the continuity equation. For the sake of brevity $\mathcal{D}_i^\rho$ is not reported here, the interested reader can find more details also in [3, 25] where the intensity of this term is determined dynamically in space and time.

The pressurer and viscous forces $\boldsymbol{F}^v$ are expressed as:

$$\begin{cases} \boldsymbol{F}_i^p := \sum_j (p_i + p_j)\,\nabla_i W_{ij}\,V_j \\[2mm] \boldsymbol{F}_i^v := K \sum_j (\mu + \mu_{ij}^T)\,\pi_{ij}\,\nabla_i W_{ij}\,V_j \qquad K := 2(n+2) \\[2mm] \pi_{ij} := \frac{\boldsymbol{u}_{ij}\cdot\boldsymbol{r}_{ij}}{\|\boldsymbol{r}_{ji}\|^2}, \quad \mu_{ij}^T := 2\,\frac{\mu_i^T\,\mu_j^T}{\mu_i^T + \mu_j^T}, \quad \mu_i^T := \rho_0\,(C_S\,l)^2\,\|\mathbb{D}_i\| \end{cases} \qquad (4)$$

where n is the number of spatial dimensions, $l = 4\Delta r$ is the radius of the support of the kernel W for two spatial dimensions and represents the length scale of the filter adopted for the LES sub-grid model. C_S is the so called Smagorinsky constant, set equal to 0.18 (see [32] and [6]). $\|\mathbb{D}\|$ is a rescaled Frobenius norm of the rate of strain tensor, namely $\|\mathbb{D}\| = \sqrt{2\mathbb{D}:\mathbb{D}}$. The viscous term (4) contains both the

effect of the physical viscosity μ as well as of the one related to the turbulent stresses μ_i^T. In order to dump the turbulent eddies near the wall boundaries a classical van Driest damping function is employed [33].

A 4th-order Runge-Kutta scheme is adopted to integrate in time system (2). The time step, Δt, is obtained as the minimum over the following bounds as set by Courant-Friedrichs-Lewy conditions:

$$\begin{cases} \Delta t_v = 0.031 \min_i \frac{l^2\,\rho_i}{(\mu + \mu_i^T)}, \quad \Delta t_a = 0.3 \min_i \sqrt{\frac{\Delta r}{\|\boldsymbol{a}_i\|}} \\[2mm] \Delta t_c = 0.6\,(l/c_0), \quad \Delta t = \min(\Delta t_v, \Delta t_a, \Delta t_c) \end{cases} \qquad (5)$$

where $\|\boldsymbol{a}_i\|$ is the particle acceleration, Δt_v is the time step related to viscosity, Δt_a is the advective time step and Δt_c is the acoustic time step (see *e.g.* [14]).

A. Enforcement of the boundary conditions

The governing equations require appropriate boundary conditions to be applied on the free surface and on the tank walls. As clarified in [10, 11], the kinematic and dynamic conditions on the free surface are intrinsically satisfied with SPH methods.

The no-slip boundary condition on the solid surface is enforced with a ghost-fluid approach (see *e.g.* [23] [4] and also [5, 28] where quasi-Lagrangian formulation is used). It requires that at least five particles should be present within the boundary layer region. High spatial resolution simulations are designed in such a way as to fulfill the above constrain.

An estimation of the boundary layer thickness (WBT) can be obtained by using the Blasius equation. Considering the Reynolds number regime studied in this work, it results that the WBT spans between 0.9 and 2.7 cm. The maximum spatial resolution adopted for the current simulations is $N = H/\Delta r = 200$, *i.e.* the particle size is 1.75 mm.

IV. Discussion on results

The present research activity considered a wide range of oscillation frequencies for the motion of the tank, at a prescribed filling depth of $h/L = 0.35$. The oscillation period T of the sinusoidal motion of the tank is made non-dimensional with the natural period of the first sloshing mode T_1. During the numerical campaign, the period T is approximately varied between $T = 0.5\,T_1$ and $T = 1.6\,T_1$. The considered amplitudes of tank motion are $A = 0.01L$, only numerical, and $A = 0.03L$ for both numerical and experimental campaign.

The experimental and numerical campaigns carried out at CNR-INM by [22] and [13] have shown that the time signals of the free surface elevation can be rather complex for some specific amplitude A or period T because of the presence of typical phenomena like wave breaking, formation of water jets, water impacts, etc. As a consequence, the wave signal maxima experience a severe scattering when doubling-frequency, tripling-period, or quasi-periodic (*i.e* periodic with a chaotic modulation) time behaviours are triggered. This means that the consideration of the highest values only, as in [29], may be
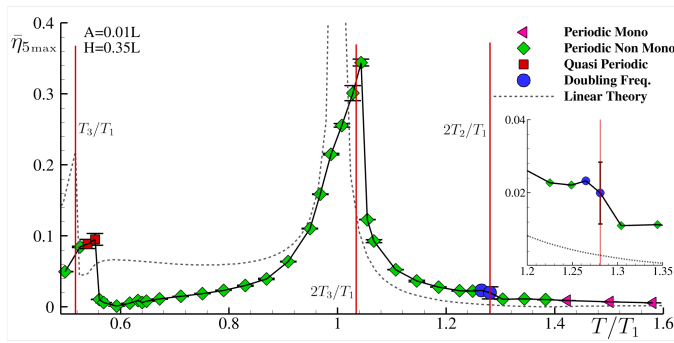
Figure 2. WEFD for tank oscillations of $0.01m$ and varying frequency. With different symbols and colors the different regimes.

not meaningful. Moreover, it should be considered that isolated spikes may occur, such distorting the data evaluation.

Following these considerations, in the present investigation the average of the maxima within a suitable time window and the associate standard deviation are taken into account. The time windows are framed after the initial transient (which usually lasts about 80 oscillation periods), where the time signal is very energetic and less significant for the description of the system behaviour.

The averaged maxima Wave Elevation Frequency Distributions (WEFD) are then built for sway oscillation amplitudes of A=1 cm and A=3 cm. For most interesting cases, Fourier spectra and phase maps are also shown.

A. Amplitude 0.01L

The experiments for oscillation amplitude of 1 *cm* are only numerical, because the physical limits of the experimental apparatus do not allow to go under 3 *cm*.

The WEFD for this oscillation amplitude, reporting the time averages of the free surface elevation maxima $\overline{\eta}_{5\max}$, is depicted in figure 2. The free surface elevation signal is analyzed after 80 oscillation periods of physical simulation time in order to avoid spurious effects from the initial transient.

As clarified in [17], the highest surface elevation is not achieved for $T = T_1$, as expected from the theoretical predictions of the linear theory described in [19], where the free surface elevation is expressed with a sine expansion.

[16] showed that the nonlinear effects modify the WEFD similarly to the *soft-spring* solutions of the Duffing equation [20] when the filling height h is greater than the critical depth (while for h lower than the critical depth the WEFD changes like an *hard-spring* solution; see *e.g.* [1, 7]).

The *soft-spring* dynamical behaviour described by [16] is discussed also in [9] for sloshing experiments near the critical depth. The amplitude response respect to the oscillation period shows two stable branches with a turning point between them. The set of turning points for different excitation amplitudes defines jumps from lower to upper branch and can be found from a cubic secular equation indicated in [16].

The WEFD resulting from linear theory is drawn in Fig. 2 with a dashed line, where the theoretical predictions are taken

from the book of [19]. The departing from the linear theory of the numerical WEFD, shown in Fig. 2, is actually due to nonlinear effects. In particular, in that figure the abscissas related to $T = T_3, 2T_3, 2T_2$ (see formula (1)) are evidenced with vertical lines.

The peak on the left side is related to the resonance of the third sloshing mode, the period of which is $T_3 = 0.517\,T_1$. The nonlinear effects lower the amplitude of $\overline{\eta}_{5\max}$ to ≈ 0.1 and shift the period to $T \approx 0.55\,T_1$.

The first sloshing mode leads to a maximum peak of WEFD observed at $T = 1.044\,T_1$ with $\overline{\eta}_{5\max} \approx 0.344$. It should be emphasized that the mode $2T_3$ is very close to the first resonance, as highlighted in Fig. 2, so that a combination between T_1 and $2T_3$ is a possible explanation of the rightward bending of the WEFD peak.

The second mode, and in general all the even modes, is not directly excited with the tank swaying, but it appears because of non linear effects. From the WEFD in Fig. 2, a little jump in the low frequency (*i.e.* long period) branch is found at $T = 2T_2$, where $T_2 = 0.64\,T_1$ is the second sloshing period. The jump is evidenced with a magnification of the WEFD in the range $T \in [1.2T_1 - 1.35T_1]$.

Once fixed the swaying amplitude, different sloshing regimes are observed at different frequencies and are indicated in Fig. 2 with different symbols (similarly to [15]). The regimes found at the smallest amplitude ($A = 0.01L$) are: periodic monochromatic, periodic non-monochromatic, doubling frequency and quasi periodic regimes.

Fig. 3 shows the time histories and the corresponding Fourier Transform spectra of η_5 for four different cases:

1)) $T = 1.50\,T_1$ Periodic Monochromatic,
2)) $T = 1.01\,T_1$ Periodic Non-Monochromatic,
3)) $T = 1.28\,T_1$ Doubling-frequency mode,
4)) $T = 0.55\,T_1$ Quasi-Periodic mode.

At low frequencies ($T > 1.4\,T_1$) η_5 behaves as a monochromatic signal. As shown in frame **(a)** of Fig. 3, the time signal resembles a simple sinusoidal function and, indeed, the Fourier transform shows a single dominant peak at $f^* = Tf = 1$. The blue circle at $f_1^* = T/T_1 = 1.50$ represents the oscillation frequency of the tank and it is dominant during the transient. In the selected time window, the latter is lower than 10^{-4}, so that it can reasonably be assumed negligible and the regime may be considered as unaffected by the transient spurious components.

Increasing the oscillation frequency, a periodic non-monochromatic time signal appears. In Fig. 3-**(b)** the signal at $T = 1.01\,T_1$, where the oscillation frequency is forced close to the first resonance, is shown. The Fourier transform shows a main peak, corresponding to the excitation frequency, at $f^* = 1$ and a sharp peak at every integer multiple.

When the excitation period T is such that $T = 2\,T_2$, the second even mode appears because of non-linear effects. This mode leads to the onset of a doubling-frequency bifurcation, clearly visible in Fig. 3-**(c)**, where the time signal η_5 presents two peaks in a period. As a consequence, a second peak at $f^* = 2$, the intensity of which is comparable to the one at
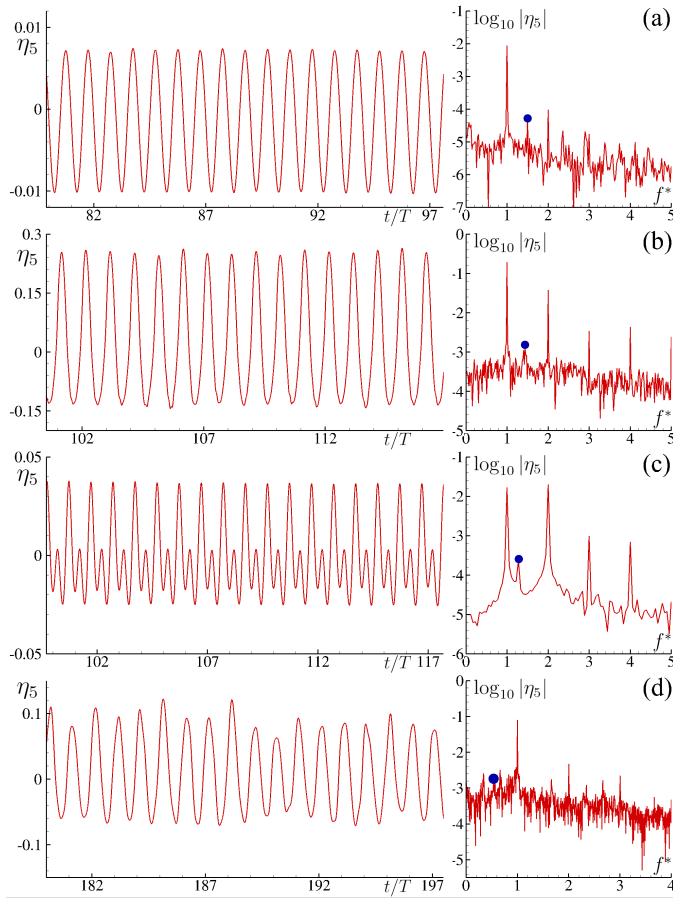
Figure 3.   Time signals (**left**) and corresponding Fourier transform spectra (**right**) for different sloshing regimes at oscillation amplitude of $0.01m$. **Frame - a**: $T/T_1 = 1.50$ - Periodic Monochromatic. **Frame - b**: $T/T_1 = 1.01$ - Periodic Non Monochromatic. **Frame - c**: $T/T_1 = 1.28$ - Doubling Frequency. **Frame - d**: $T/T_1 = 0.55$ - Quasi Periodic. The non-dimensional frequency is $f^* = Tf$. The blue circles indicates the amplitudes related to first natural frequency $f_1^* = T/T_1$.

$f^* = 1$, occurs in the Fourier transform. Similarly, nonlinear effects induce a similar behaviour for $f^* = 3$ and $f^* = 4$.

At high frequency, when the period T is close to T_3, a quasi-periodic regime is achieved. A quasi-periodic signal is a periodic signal modulated by a chaotic component (see *e.g.* [15]). In Fig. 3-(**d**), the time signal and the Fourier transform of η_5 is shown at $T = 0.55T_1$. The Fourier transform presents a dominant peak for $f^* = 1$ while the rest of the spectrum is continuous, typical of chaotic signals (see *e.g.* [15]).

The final motion of the tank is attained after a ramp, during which, besides the forcing frequency $1/T$, a continuous spectrum of modes is excited. The 1st natural mode (*i.e.* the first resonance) of period T_1 is the most energetic (among them) during the initial transient stage, whereas the other ones typically weaken rather quickly, unless strengthened by mutual nonlinear interactions. In fact, the 1st natural mode behaves alike a modulation of the time signals that, in same cases, decays after long transients during which the corresponding component remains as a distinct peak in the Fourier spectrum.
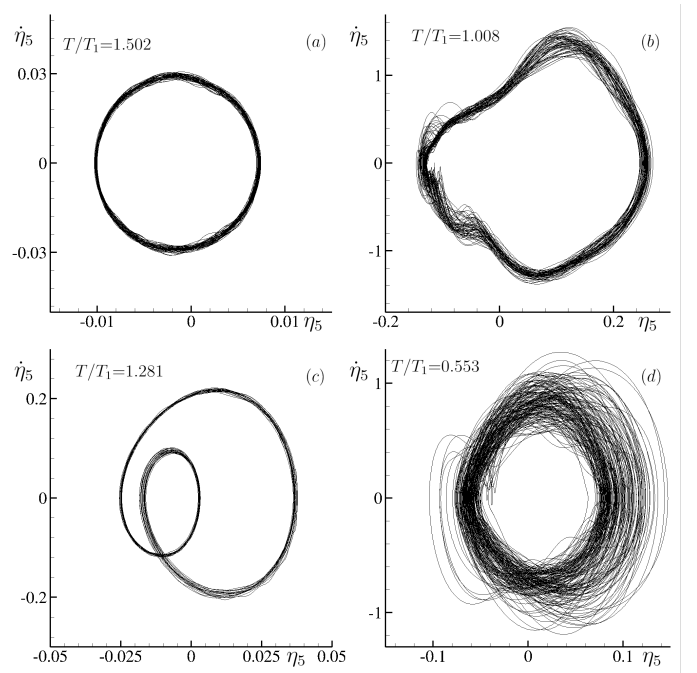
Figure 4.   Phase maps for different sloshing regimes at oscillation amplitude of $0.01m$. Cases (a) and (d) of Fig. 3 on the **left** frame and and cases (b) and (c) on the **right** frame.

In order to show that the simulations are long enough to make negligible this effect within the analysed time windows, a blue-dot corresponding to the amplitude of the 1st natural mode is drawn in the Fourier spectra of Fig. 3. As visible, it is always associated to amplitudes of about 2 orders of magnitude lower than the amplitude of the excitation frequency.

Fig. 4 depicts the phase maps $(\eta_5, \dot{\eta}_5)$. For the case a) the periodic monochromatic signal is represented, as expected, by an elliptical orbit in Fig. 4 - **(a)**. The frame **(b)** of Fig. 4 reports the phase map of the case b), where the periodic non-monochromatic behaviour leads to an orbit which is an elliptical shape distorted by the non-linearities. The thickness of the set of curves indicates the presence of a weak modulation that does not preserve a single stable orbit. The doubling frequency regime of case c) is represented in Fig. 4-**(c)** by a knotted orbit with the internal little loop related to the lower peak within the signal period. The quasi-periodic phase map, case d), is shown in Fig. 4-**(d)** and is characterized by nearly circular orbits, where the unpredictable amplitude modulation gives rise to a severe scattering of them.

B. Amplitude 0.03L

Experimental and numerical campaigns have been carried out for $A = 0.03L$. The numerical and experimental WEFD are drawn in Fig. 5, together with the different regimes identification, given coherently with the classification of section IV-A. As a comparison, the theoretical WEFD coming from multimodal approach of [16] is superimposed to the experimental and numerical results.

Figure 5. WEFD for tank oscillations of $0.03m$ and varying frequency. With different symbols and colors the different regimes. **Top**: numerical simulations. **Bottom**: experiments.
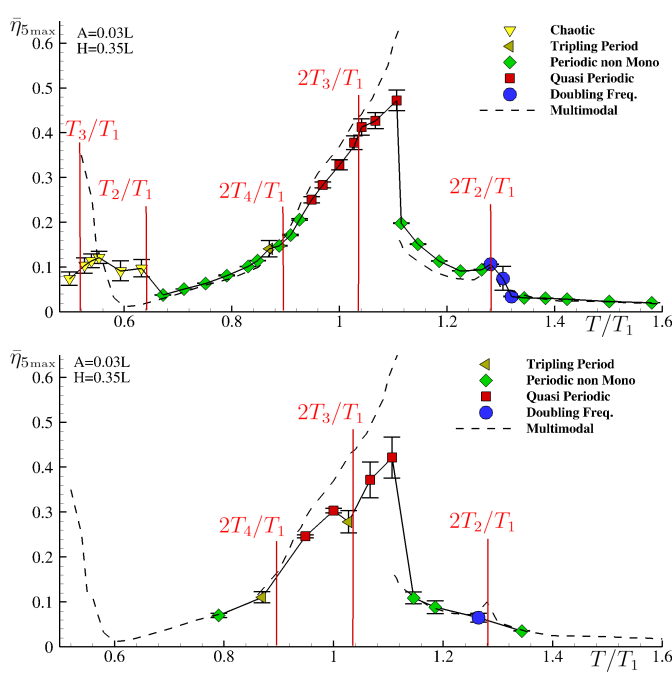
The theoretical approach is not capable to take into account singular events as breaking or wave impacts, so the high frequency cases are not properly predicted. Despite of it, as visible by the dashed line of top frame of Fig. 5, the numerical results are rather close to multimodal data, at least in the range $T/T_1 \in [0.67 - 1.6]$. Regardless its intrinsic limitations, the multimodal approach is able to predict the bifurcation around $T = 1.1\,T_1$ and the doubling frequency jump at $T = 2\,T_2$. Conversely, the numerical outcomes reveal a chaotic wave height time signal in the range $T/T_1 \in [0.50 - 0.67]$, where the multimodal solution shows a high peak related to the third resonance T_3/T_1 and is thus unable to predict such a behaviour.

Bottom plot of Fig. 5 reports the comparison between with the experimental data and the multimodal approach. In the
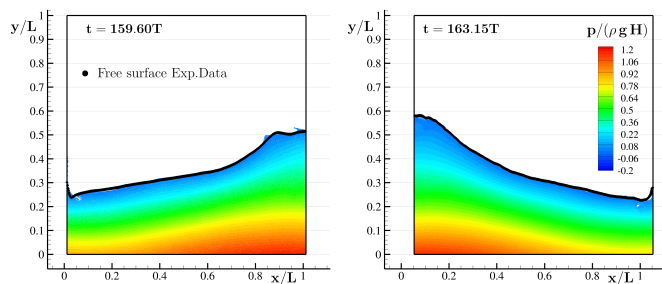

Figure 6. Test case A = 0.03L, $T/T_1 = 0.944$, corresponding to a quasi-period regime. Colors are representative of the δ-LES-SPH pressure field. Black dots are the free surfaces extracted by the experimental video

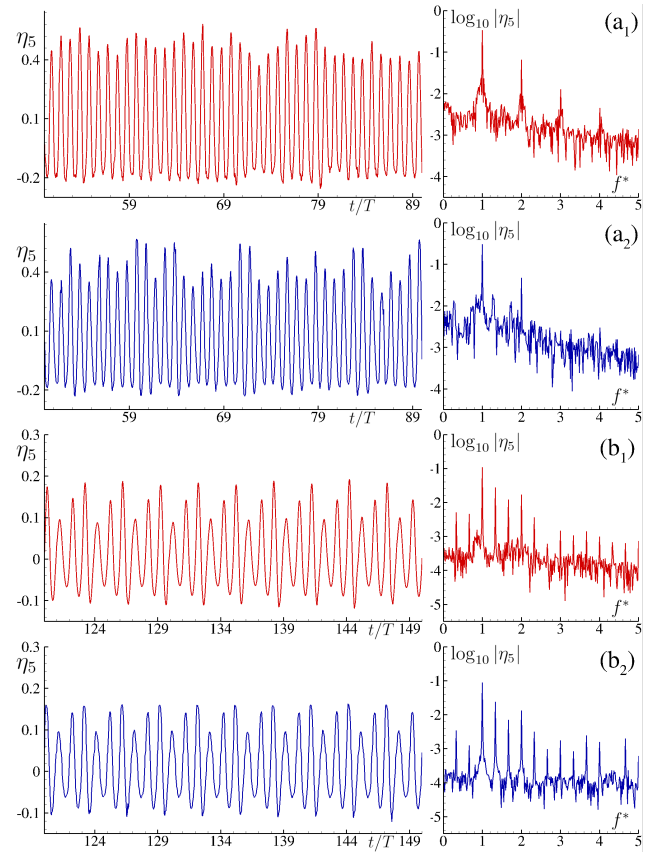period ranges $T/T_1 \in (0.79, 1.00)$ and $T/T_1 \in (1.14, 1.34)$ the

Figure 7. Time signals (**left**) and corresponding Fourier transform spectra (**right**) for different sloshing regimes at oscillation amplitude of $0.03m$. **Frame - a_1**: $T/T_1 = 1.10$ - Quasi periodic - numerical simulations. **Frame - a_2**: $T/T_1 = 1.10$ - Quasi periodic - experiments. **Frame - b_1**: $T/T_1 = 0.867$ - Tripling period - numerical simulations. **Frame - a_2**: $T/T_1 = 0.867$ - Tripling period - experiments. The non-dimensional frequency is $f^* = Tf$.

numerical results are in a good agreement with the experimental data in terms of mode classification, value of $\bar{\eta}_{5max}$ and its related standard deviation. In particular, the doubling-frequency regime is found experimentally and numerically near $T = 2T_2$ similarly to amplitude $A = 0.01L$, already discussed in section IV-A. At $T = 0.867\,T_1$ a tripling-period bifurcation is identified by both δ-LES-SPH and experiments.

In order to stress better the similitude between numerical predictions and experimental data, Fig. 6 compares the free surface extracted from camera acquisition with the δ-LES-SPH particle configuration at $T = 0.944T_1$. Two different time instants were considered, corresponding to most leftward and most rightward tank positions. The agreement is rather good with small discrepancies mainly linked to breaking events typical of the quasi-periodic regime.

Although the experimental/numerical comparisons are generally in good accordance, at $T = 2T_3$ the experiments show a second tripling-period scenario not found with the numerical simulations. The disagreement is mainly related to 3D effects, in fact the fragmentation of the free surface is more intense in the experiments than in the 2D simulations. Indeed, the
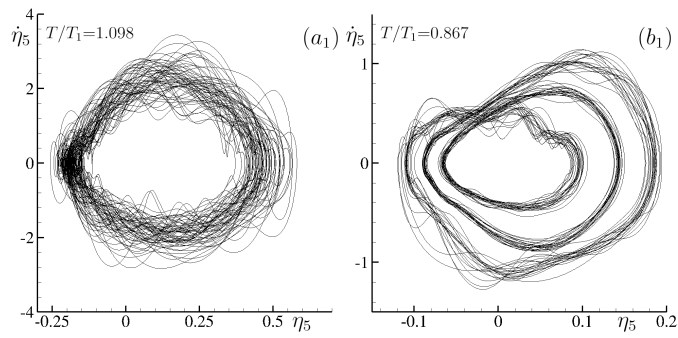
Figure 8.   Phase maps for different sloshing regimes from numerical simulations at oscillation amplitude of 0.03L. **Frame - a$_1$**: Quasi-periodic. **Frame - b$_1$**: Tripling-period.
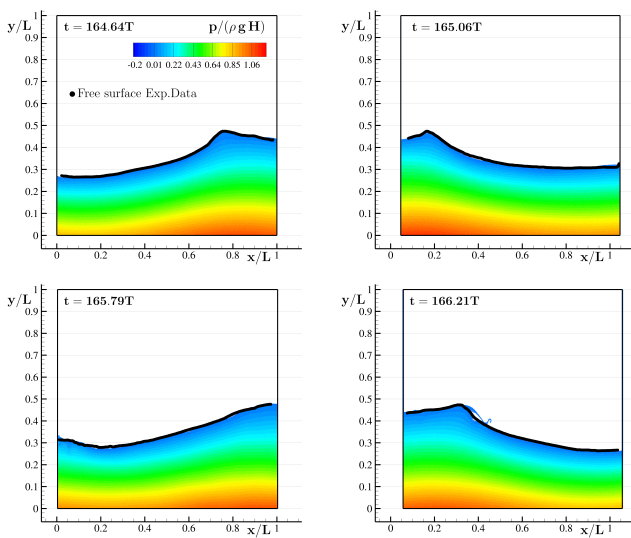

Figure 9.   Test case $A = 0.03L$, $T/T_1 = 0.867$, corresponding to a tripling-period regime. Colors are representative of the δ-LES-SPH pressure field. Black dots are the free surfaces extracted by the experimental video.

peaks which lead to a larger standard deviation for δ-LES-SPH. The tripling-period mode is characterized by a periodic sequence with period $3T$ characterized by three local maxima. This behaviour reflects on the Fourier transform where, beside the peak at the excitation period T, two other peaks at lower frequency appears. The non-linear combination of three frequency components excite also other high frequency harmonics, such leading to the peaked shape of the Fourier spectra.

Phase maps $(\eta_5, \dot{\eta}_5)$ related to the former regimes are depicted in Fig. 8. In the left plot of Fig. 8 a quasi-periodic map is drawn for $T = 1.107\,T_1$. The orbit related to the excitation period T is disturbed by chaotic modulation and the final orbit appears rather scattered with evident fluctuations. In the right plot of the same figure, the tripling-period regime at $T = 0.867\,T_1$ is characterized by three concatenate orbits. Again the orbits are characterized by scattering and fluctuations which are related to breaking wave events.

For this latter case, Fig. 9 depicts the free-surface extracted by camera acquisition and compares it with the simulation SPH particles at four time instants, demonstrating a fair good agreement between them. It is worth noting that in the δ-LES-SPH plunging breaking waves are developed, while in the experiments only spilling breakers are found. These differences are likely related to the fact that the surface tension effects are neglected in the numerical model.

REFERENCES

[1] M. Antuono, B. Bouscasse, A. Colagrossi, and C. Lugni. Two-dimensional modal method for shallow-water sloshing in rectangular basins. *Journal of Fluid Mechanics*, 700:419–440, 2012.

[2] M. Antuono, A. Colagrossi, and S. Marrone. Numerical diffusive terms in weakly-compressible SPH schemes. *Computer Physics Communications*, 183(12):2570–2580, 2012.

[3] M. Antuono, S. Marrone, A. Di Mascio, and A. Colagrossi. Smoothed particle hydrodynamics method from a large eddy simulation perspective. generalization to a quasi-lagrangian model. *Physics of Fluids*, 33(1):015102, 2021.

[4] M. Antuono, C. Pilloton, A. Colagrossi, and D. Durante. Clone particles: A simplified technique to enforce solid boundary conditions in SPH. *Computer Methods in Applied Mechanics and Engineering*, 409:115973, 2023.

[5] M. Antuono, P.N. Sun, S. Marrone, and A. Colagrossi. The δ-ALE-SPH model: An arbitrary lagrangian-eulerian framework for the δ-SPH model with particle shifting technique. *Computers & Fluids*, 216:104806, 2021.

fragmentation induces extra-dissipation phenomena which are responsible for the lower value of $\bar{\eta}_5$. Similarly, the highest points of the WEFD at $T = 1.067T_1$ and $T = 1.107T_1$ of the experimental data are about the 13% lower than the δ-LES-SPH results.

Fig. 7 shows the experimental and numerical time histories and the related Fourier transforms for case $T = 1.107\,T_1$ (frames a$_1$ and a$_2$) and $T = 0.867\,T_1$ (frames b$_1$ and b$_2$). As commented above, the numerical simulation represented in frame (**a$_1$**) presents a more energetic signal with respect to the experimental one, shown in frame (**a$_2$**). A quasi-periodic regime is attained for both signals, as evidenced by the Fourier spectrum, where dominant peaks overlies an almost continuous spectrum, as it is typical of a chaotic modulation.

The case $T = 0.867\,T_1$, close to the period $T = 2\,T_4$, corresponds to a tripling-period scenario. The numerical and experimental time histories are reported in the frames (**b$_1$**) and (**b$_2$**) of Fig. 7, respectively. The signals look very similar although some differences are visible in the height of the

[6] C. Bailly and G. Comte-Bellot. *The Dynamics of Isotropic Turbulence*, pages 179–210. Springer International Publishing, 2015.

[7] B. Bouscasse, M. Antuono, A. Colagrossi, and C. Lugni. Numerical and experimental investigation of nonlinear shallow water sloshing. *International Journal of Nonlinear Sciences and Numerical Simulation*, 14(2):123–138, 2013.

[8] B. Bouscasse, A. Colagrossi, G. Colicchio, and C. Lugni. Numerical and experimental investigation of sloshing phenomena in conditions of low filling ratios. In *Proc. 10th Numerical Towing Tank Symposium (NuTTS'07) Hamburg, Germany*, pages 23–25, 2007.

[9] A. Colagrossi. A meshless lagrangian method for free-surface and interface flows with fragmentation. *Ph.D. Thesis, Università di Roma*, 2005.

[10] A. Colagrossi, M. Antuono, and D. Le Touzé. Theoretical considerations on the free-surface role in the smoothed-particle-hydrodynamics model. *Physical Review E*, 79(5):056701, 2009.

[11] A. Colagrossi, M. Antuono, A. Souto-Iglesias, and D. Le Touzé. Theoretical analysis and numerical verification of the consistency of viscous smoothed-particle-hydrodynamics formulations in simulating free-surface flows. *Physical Review E*, 84(2):026705, 2011.

[12] A. Colagrossi, C. Lugni, M. Greco, and O.M. Faltinsen. Experimental and numerical investigation of 2D sloshing with slamming. In *Proc. 19th Int. Workshop on Water Waves and Floating Bodies, Cortona, Italy*, 2004.

[13] A. Colagrossi, F. Palladino, M. Greco, C. Lugni, and O.M. Faltinsen. Experimental and numerical investigation of 2d sloshing with slamming: scenarios near the critical filling depth. In *Proc. 21st Int. Workshop on Water Waves and Floating Bodies, Cortona, Italy*, 2006.

[14] A. Colagrossi, E. Rossi, M. Marrone, and D. Le Touzé. Particle methods for viscous flows: analogies and differences between the SPH and DVH methods. *Communications in Computational Physics*, 20(3):660–688, 2016.

[15] D. Durante, O. Giannopoulou, and A. Colagrossi. Regimes identification of the viscous flow past an elliptic cylinder for Reynolds number up to 10000. *Communications in Nonlinear Science and Numerical Simulation*, 102:105902, 2021.

[16] O.M. Faltinsen, O.F. Rognebakke, I.A. Lukovsky, and A.N. Timokha. Multidimensional modal analysis of nonlinear sloshing in a rectangular tank with finite water depth. *Journal of fluid mechanics*, 407:201–234, 2000.

[17] O.M. Faltinsen and A.N. Timokha. An adaptive multimodal approach to nonlinear sloshing in a rectangular tank. *Journal of Fluid Mechanics*, 432:167–200, 2001.

[18] O.M. Faltinsen and A.N. Timokha. *Sloshing*. Cambridge University Press, 2009.

[19] R.A. Ibrahim. *Liquid sloshing dynamics: theory and applications*. Cambridge University Press, 2005.

[20] I. Kovacic and M.J. Brennan. *The Duffing equation: nonlinear oscillators and their behaviour*. John Wiley & Sons, 2011.

[21] S.J. Lind, R. Xu, P.K. Stansby, and B.D. Rogers. Incompressible smoothed particle hydrodynamics for free-surface flows: A generalised diffusion-based algorithm for stability and validations for impulsive flows and propagating waves. *Journal of Computational Physics*, 231(4):1499–1523, 2012.

[22] C. Lugni, G. Colicchio, and A. Colagrossi. Investigation of sloshing phenomena near the critical filling depth through the hilbert-huang transformation. In *Proc. 9th Numerical Towing Tank Symposium (NuTTS'06) Le Croisic, France*, pages 89–94, 2006.

[23] F. Macia, M. Antuono, L.M. González, and A. Colagrossi. Theoretical analysis of the no-slip boundary condition enforcement in sph methods. *Progress of theoretical physics*, 125(6):1091–1121, 2011.

[24] S. Marrone, A. Colagrossi, F. Gambioli, and L. González-Gutiérrez. Numerical study on the dissipation mechanisms in sloshing flows induced by violent and high-frequency accelerations. I. theoretical formulation and numerical investigation. *Physical Review Fluids*, 6:114801, 2021.

[25] D.D. Meringolo, S. Marrone, A. Colagrossi, and Y. Liu. A dynamic δ-sph model: How to get rid of diffusive parameter tuning. *Computers & Fluids*, 179:334–355, 2019.

[26] J. Michel, D. Durante, A. Colagrossi, and S. Marrone. Energy dissipation in violent three-dimensional sloshing flows induced by high-frequency vertical accelerations. *Physics of Fluids*, 34(10):102114, 2022.

[27] R.M. Nestor, M. Basa, M. Lastiwka, and N.J. Quinlan. Extension of the finite volume particle method to viscous flow. *Journal of Computational Physics*, 228(5):1733–1749, 2009.

[28] G. Oger, S. Marrone, D. Le Touzé, and M. De Leffe. SPH accuracy improvement through the combination of a quasi-Lagrangian shifting transport velocity and consistent ALE formalisms. *Journal of Computational Physics*, 313:76–98, 2016.

[29] H. Olsen. Unpublished sloshing experiments at the technical university of delft. *Delft, The Netherlands*, 1970.

[30] O.F. Rognebakke and O.M. Faltinsen. Sloshing induced impact with air cavity in rectangular tank with a high filling ratio. In *20th International Workshop on Water Waves and Floating Bodies, Spitsbergen, Norway*, 2005.

[31] S. Silverman and H.N. Abramson. The dynamic behavior of liquids in moving containers. *NASA SP-106*, pages 13–78, 1966.

[32] J. Smagorinsky. General circulation experiments with the primitive equations: I. the basic experiment. *Monthly weather review*, 91(3):99–164, 1963.

[33] E.R. Van Driest. On turbulent flow near a wall. *Journal of the aeronautical sciences*, 23(11):1007–1011, 1956.